

## Factors that inhibit snowball Earth simulation

C. J. Poulsen

Department of Geological Sciences, University of Michigan, Ann Arbor, Michigan, USA

R. L. Jacob

Argonne National Laboratory, Argonne, Illinois, USA

Received 24 May 2004; revised 23 August 2004; accepted 11 October 2004; published 9 December 2004.

[1] A coupled ocean-atmosphere general circulation model with a thermodynamic sea-ice model, the Fast Ocean Atmosphere Model version 1.5, is used to investigate the factors that inhibit the simulation of global sea ice. In the control experiment with reduced solar luminosity (93% of modern), low atmospheric pCO<sub>2</sub> (140 ppm), and an idealized tropical continent, the sea-ice margin equilibrates at ~27° latitude. A series of experiments was completed to systematically test the influence of deep-ocean circulation, wind-driven ocean circulation, convective mixing, sea-ice treatment, and radiative-cloud forcing, on the sea-ice extent. Model results indicate that both wind-driven circulation and cloud-radiative forcing are critical factors that inhibit sea-ice advance into the low latitudes. The wind-driven ocean circulation transports heat to the sea-ice margin, stabilizing the sea-ice margin. Clouds yield a positive radiative forcing over ice, warming the air overlying sea ice and decreasing sensible heat loss at the sea-ice margin. In the absence of either factor, sea ice expands to the equator within 15 model years, yielding a snowball Earth. We also find that intensification of the Hadley circulation as sea ice enters the Hadley domain promotes the climate instability that leads to global sea-ice cover. Results from this study help explain the wide disparity in conditions necessary to simulate global ice cover in previous climate models of the Neoproterozoic. *INDEX TERMS:* 3337 Meteorology and Atmospheric Dynamics: Numerical modeling and data assimilation; 3344 Meteorology and Atmospheric Dynamics: Paleoclimatology; 4267 Oceanography: General: Paleoclimatology; 9619 Information Related to Geologic Time: Precambrian; *KEYWORDS:* Neoproterozoic, snowball Earth, paleoclimate

**Citation:** Poulsen, C. J., and R. L. Jacob (2004), Factors that inhibit snowball Earth simulation, *Paleoceanography*, 19, PA4021, doi:10.1029/2004PA001056.

### 1. Introduction

[2] The possibility that Earth was completely ice-covered in the late Neoproterozoic era, about 750 and 610 millions years ago, is one of the most provocative theories in the Earth sciences. The geological evidence for a snowball Earth has been vigorously debated. Champions of the snowball Earth hypothesis point to unusual features in the geologic record including the existence of low-latitude diamictites and lonestones, anomalies in the C-isotopic reservoir, the unusual presence of “cap carbonates” atop diamictites, and the occurrence of banded iron formation, as evidence for global glaciation and its aftermath [Kirschvink, 1992; Hoffman *et al.*, 1998; Hoffman and Schrag, 2002]. Critics of the snowball Earth hypothesis refute this interpretation of the geological evidence. Most recently, Eyles and Januszczak [2004] argue that many of the Neoproterozoic diamictites were the product of tectonically driven, diachronous, nonglacial, subaqueous mass flow processes in marine basins. In addition, alternative interpretations have been offered for the genesis of banded iron formations, C-isotopic excursions, and cap carbonates that do not require global ice cover [Kennedy *et al.*, 2001; Jiang *et al.*, 2003; Ridgwell *et al.*, 2003].

[3] In theory, climate models should be well suited for testing the snowball Earth hypothesis. The magnitude of the response (global glaciation) is seemingly large enough to render nuances of the climate system unimportant. Perhaps for this reason a hierarchy of climate models, ranging from energy balance models to ocean-atmosphere general circulation models, has been employed to evaluate Earth’s susceptibility to global glaciation. However, climate models offer no consensus on a Neoproterozoic snowball Earth; the critical CO<sub>2</sub> value for global sea-ice cover has been reported to be as low as 89 ppm in an intermediate complexity climate model [Donnadieu *et al.*, 2004] and as high as 1800 ppm in a sophisticated energy balance model [Lewis *et al.*, 2003] with a 6% reduction in modern solar luminosity. While many models exhibit strong climate instability with the advance of sea ice into the low latitudes, some models support the possibility of a partially ice-covered ocean [Hyde *et al.*, 2000; Chandler and Sohl, 2000; Poulsen, 2003].

[4] In comparison to many climate model simulations of the Neoproterozoic, late Neoproterozoic simulations using a coupled ocean-atmosphere model, the Fast Ocean Atmosphere Model (FOAM), have demonstrated a resistance to global sea-ice coverage [Poulsen *et al.*, 2001, 2002]. This behavior has been attributed to the transport of heat to the sea-ice margin by the ocean [Poulsen *et al.*, 2001]. In this study, we use FOAM with a thermodynamic sea-ice model

**Table 1.** Summary of FOAM1.5 Modeling Experiments and Results

Experiment	Run Length, years	Description	Result
FC	400	atmosphere GCM was coupled to an ocean GCM and the 3-level Semtner-sea-ice model	sea-ice line to 27°
FC_SICE	40	a very simple, nonthermodynamic sea-ice model was implemented in place of the thermodynamic sea-ice model in FC	sea-ice line to 60° with large seasonal fluctuations
FC_NCNV	100	ocean convective adjustment parameterization was disabled, eliminating buoyancy adjustments	sea-ice line to 27°
FC_NWND	20	wind-forcing on the ocean from the atmosphere was turned off, effectively stopping wind-driven ocean circulation	global sea-ice cover
FC_NCLD	20	radiative effects of clouds in the atmosphere GCM were disabled	global sea-ice cover
FC_SHLW	100	ocean bathymetry was uniformly specified as 86 m	sea-ice line to 24°
FC_92SL	100	same configuration as FC, but with solar luminosity 92% of modern	sea-ice line to 26°
FC_91SL	57	same configuration as FC, but with solar luminosity 91% of modern	global sea-ice cover
SLAB	20	atmosphere GCM was coupled to a 50 m mixed layer ocean model with no ocean heat transport	global sea-ice cover

to explore the climate factors that inhibit global sea-ice cover. By systematically “turning off” elements of the climate, we determine that the wind-driven ocean circulation and cloud radiative forcing are the two factors that are most important in stopping the ice albedo feedback in FOAM. This study also illustrates that the large disparity in previous modeling results can be explained by their disparate capabilities.

## 2. Methodology

[5] To determine the factors that inhibit a snowball Earth, we used FOAM 1.5, a fully coupled ocean-atmosphere GCM [Jacob, 1997]. The atmospheric component of FOAM is a parallel version of CCM3 [Kiehl *et al.*, 1996] created with the two-dimensional parallel version of CCM2 [Drake *et al.*, 1995] and updated with the CCM3 physics [Jacob, 1997]. The atmosphere runs at R15 spectral resolution ( $4.5^\circ \times 7.5^\circ$ ) with 18 levels. The ocean component of FOAM is a 24-level ocean GCM on a  $128 \times 128$  point Mercator grid ( $1.4^\circ \times 2.8^\circ$ ). In contrast to earlier Neoproterozoic studies using FOAM [Poulsen *et al.*, 2001, 2002; Poulsen, 2003], the sea-ice component in version 1.5 of FOAM uses the thermodynamic component of the sea-ice model in CSM1.4, which is based on the Semtner 3-layer thermodynamics snow/ice model [Semtner, 1976]. There is still no sea-ice dynamics in FOAM 1.5. In our version of FOAM 1.5, we have adjusted a parameter in the sea-ice model to provide a reasonable simulation of Last Glacial Maximum sea-ice distribution. Without this adjustment, the LGM sea ice is far too extensive reaching southern Australia and well into the North Pacific.

[6] The FOAM experiments have identical boundary conditions, except as noted below and in Table 1. All experiments include an idealized supercontinent centered on the equator with the radiative characteristics of a desert

(albedo of 0.35 and 0.51 in the visible and near-infrared wavelengths). Our purpose in implementing the idealized paleogeography was to maximize tropical continental area, an important factor if drawdown of atmospheric  $\text{CO}_2$  through silicate weathering triggered ice cap instability [Marshall *et al.*, 1988]. The land surface in the model has the radiative characteristics of a desert because land plants had yet to evolve in the Neoproterozoic. At 600 Ma, the solar luminosity was between 4.7% and 6.3% lower than at present [Crowley and Baum, 1993]. To facilitate snowball conditions, a 7.0% reduction in the solar constant, a  $\text{CO}_2$  value of 140 (ppmv), and preindustrial  $\text{CH}_4$  concentration of 700 (ppbv) were specified. In two experiments, FC\_91SL and FC\_92SL, the solar luminosity was reduced to 92 and 91% of modern ( $1367 \text{ Wm}^{-2}$ ). The model eccentricity, obliquity, precession, rotation rate, and ozone concentrations were defined as modern values. The ocean has a uniform depth of 5500 m except in the FC\_SHLW experiment, which had an ocean depth of 86 m. Initial conditions were similar in all but the SLAB experiment. In all FC-type experiments (Table 1), the ocean was initialized with a uniform salinity (34.9 psu) and the following ocean temperature profile: 0.0 °C (0–20 m), –0.5 °C (21–40 m), –1.0 °C (41–86 m), –1.5 °C (87–145 m), and –1.8 °C (146–5500 m). In the SLAB experiment, run with a 50-m mixed layer ocean model, the ocean temperatures were uniformly initialized as 20°C.

[7] In this study, FOAM was run with a number of modifications to determine what elements of the ocean-atmosphere model were critical to preventing a snowball Earth. The control experiment, FC, is a standard FOAM run with Neoproterozoic initial and boundary conditions as described above. In all other experiments, a single modification or parameter change was made. The FC experiment was integrated for 400 years; the FC\_SICE experiment was run for 40 years (see simple sea-ice model for explanation);

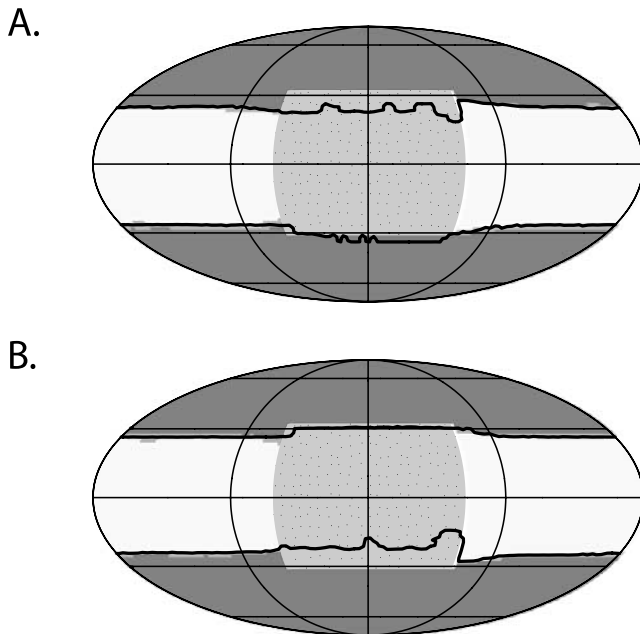


**Figure 1.** Average sea-ice fraction in (a) December, January, and February and (b) June, July, and August. The Neoproterozoic continent is filled with a gray dotted pattern; ice-free ocean is not shaded. Year-round sea ice is shaded dark gray; seasonal ice is shaded light gray. The thick, black contour line marks snow accumulation of more than 0.1 m. The sea-ice line equilibrated at  $\sim 27^\circ$  latitude with small seasonal variations. Only the poleward edge of the continent sustains annual snow accumulation. The sea-ice fraction and snow thickness data represent the average of the last 10 years of the FC simulation (years 391–400).

all other experiments were integrated for 100 years or until global ice cover was achieved. Table 1 describes the nine experiments and the consequent sea-ice response.

### 3. Climate Model Results

#### 3.1. Control Experiment

[8] As in previous FOAM experiments [Poulsen *et al.*, 2001], the control experiment does not simulate global ice coverage. The sea-ice line stabilizes at  $\sim 27^\circ$  latitude with small seasonal fluctuations of  $\sim 3^\circ$  (Figure 1). The sea-ice line also exhibits multidecadal variability (Figure 2a). Snow accumulates on sea ice and the poleward edge of the continent. On a seasonal basis, snow accumulates on the continent to  $\sim 18^\circ$  but is not maintained year-round. Seasonal sea-surface temperatures range from  $12.5^\circ\text{C}$  at low latitudes to  $-100^\circ\text{C}$  at the poles (Figure 3). Seasonal continental surface temperatures range from just above freezing to less than  $-25^\circ\text{C}$ .

[9] The FC experiment was integrated for 400 years without any acceleration of the deep ocean. Throughout the integration, the global ocean warmed at a rate of  $0.07^\circ\text{C}/100$  years. Most of the warming occurred in the upper 1500 m with slight warming in the deeper ocean. The heat content of the tropical and subtropical upper ocean

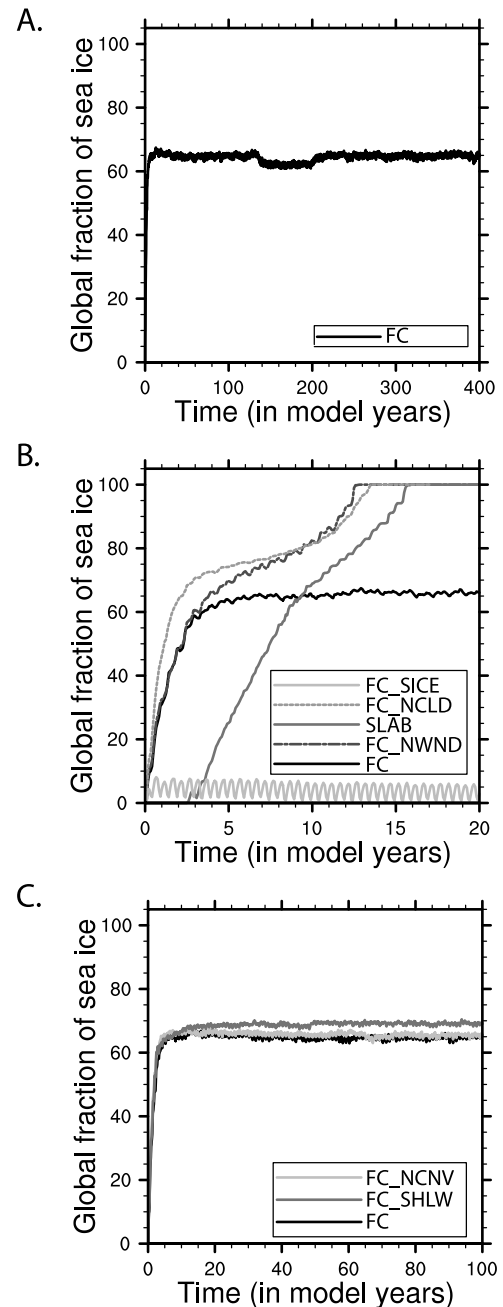


**Figure 2.** Global average sea-ice fraction versus time (model years). (a) The global ice fraction in the 400 year FC experiment. The global ice fraction equilibrates at  $\sim 27^\circ$  latitude with no long-term trend. The ice fraction exhibits multidecadal variability with a slight decrease in ice fraction between years 130 and 210. (b) The evolution of the global ice fraction in the FC, FC\_NWND, SLAB, FC\_NCLD, and FC\_SICE experiments. Note that the global ice fraction for the SLAB experiment lags the FC-type experiments because the initial ocean temperatures were greater. (c) The evolution of the global ice fraction in the FC, FC\_NCNV, and FC\_SHLW experiments after 100 model years. In all three experiments the sea-ice margin stabilizes between  $\sim 27^\circ$  and  $\sim 24^\circ$  latitude.

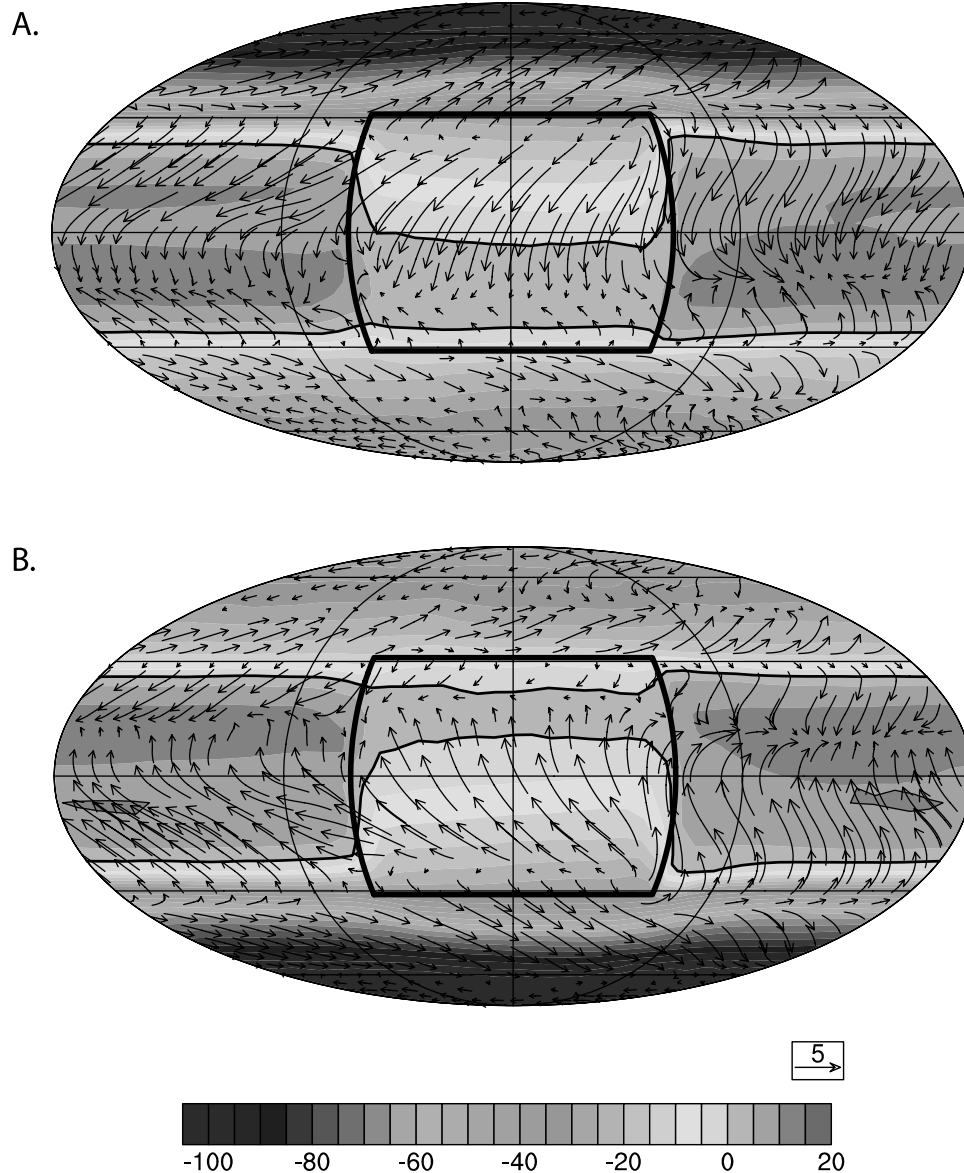


**Figure 3.** (a) December, January, and February and (b) June, July, and August surface temperature ( $^{\circ}\text{C}$ ) and 993-mb wind vectors ( $\text{m}^2\text{s}^{-2}$ ) in the FC. Maximum surface temperatures exceed  $12.5^{\circ}\text{C}$  in the subtropical ocean. Polar temperatures vary from approximately  $-100^{\circ}\text{C}$  in winter to  $-40^{\circ}\text{C}$  in summer. The wind vectors illustrate a large, seasonal cross-equatorial flow through the trade winds. The surface temperature and wind data were average over the last 10 years of the FC experiment (years 391–400). The thick, solid line outlines the Neoproterozoic continent. See color version of this figure in the HTML.

increased significantly over the course of the run (Figure 4). On the basis of the substantial warming in the upper ocean, it is unlikely that further model integration will lead to global ice cover.

[10] Examining the heat budget at  $23^{\circ}\text{N}$ , located in front (equatorward) of the sea-ice line, provides insight into why the sea-ice advance stopped near  $27^{\circ}$ . The local energy balance between the total radiation, latent and sensible heat fluxes, ocean heat transport, and heat exchanged in the formation and melting of ice determines the equilibrium sea-ice position. Figure 5 illustrates the energy balance at  $23^{\circ}\text{N}$  as the sea-ice line migrates toward the low latitudes.

During the first 12 years, as high-latitude temperatures decrease, the sensible heat flux increases by more than  $120\text{ Wm}^{-2}$ . Increased ocean heat transport and reduced latent heat flux partially compensate for the large sensible heat flux loss, but the total heat flux is negative ( $>-5\text{ Wm}^{-2}$ ) yielding a temperature decrease of  $7^{\circ}\text{C}$ . By year 12, the sea-ice line is near equilibrium. At  $23^{\circ}\text{N}$ , the ocean gains heat through radiation ( $\sim 100\text{ Wm}^{-2}$ ) and ocean heat transport ( $\sim 130\text{ Wm}^{-2}$ ) and loses heat through latent ( $\sim 90\text{ Wm}^{-2}$ ) and sensible ( $\sim 140\text{ Wm}^{-2}$ ) heat fluxes to the atmosphere.

[11] As demonstrated in Figure 5, the ocean heat transport increases by  $\sim 170\text{ Wm}^{-2}$  through the first 12 years of the

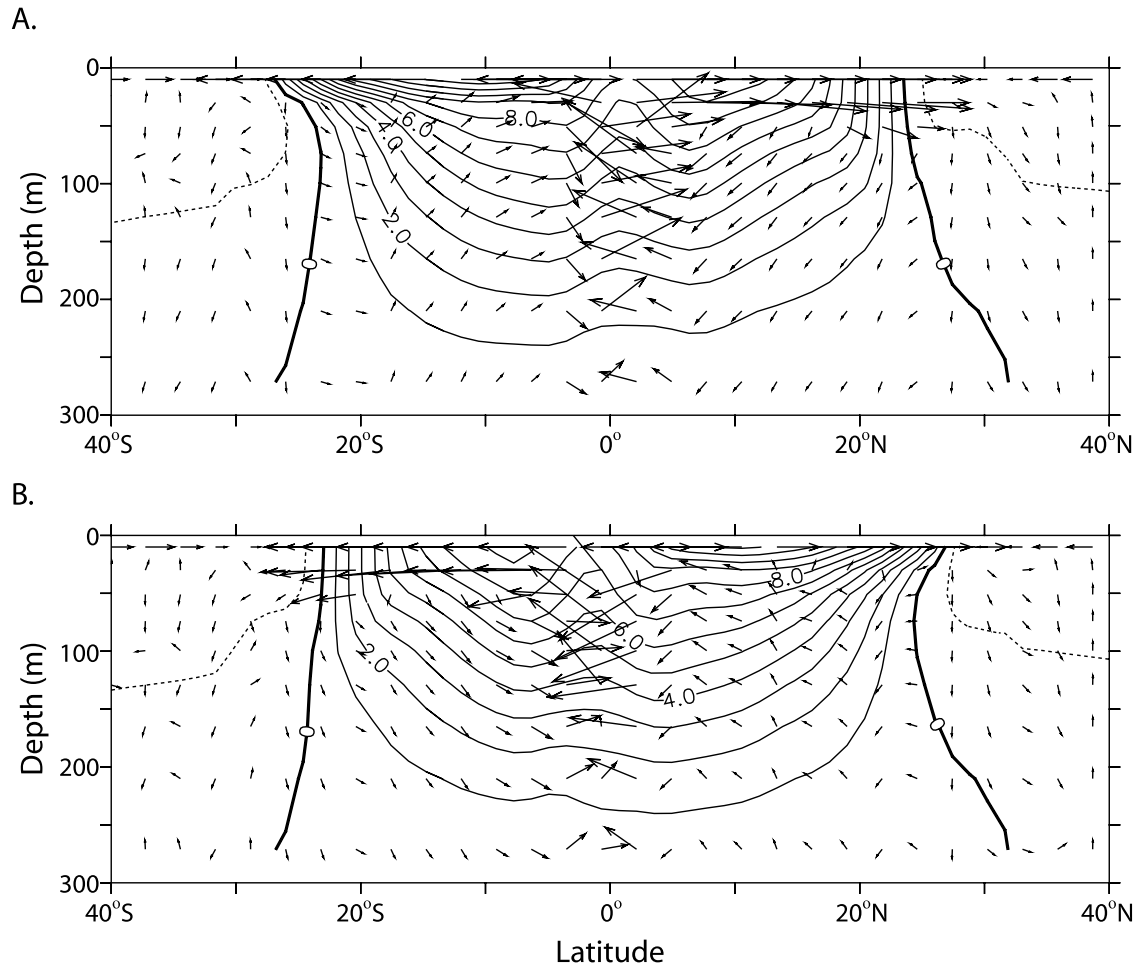


**Figure 4.** Zonally average meridional flow ( $\text{m}^2\text{s}^{-2}$ ) and temperature ( $^{\circ}\text{C}$ ) in the upper ocean during (a) January and (b) July. Velocity vectors display the mean meridional flow. For display purposes the vertical component of the velocity vectors has been scaled by  $\sim 1000$ . Note the large cross-equatorial surface flow into the winter hemisphere and the subsurface return flow. The data were averaged over the last 10 years of the FC experiment (years 391–400).

model run and is largely responsible for counterbalancing sensible heat loss near the sea-ice margin. The wind-driven circulation most likely drives this ocean heat transport (see section 3.6). The upper ocean has a strong overturning circulation that moves warm water from the low latitudes toward the sea-ice margin (Figure 4). The ocean heat transport is approximately 2.5 PW near the sea-ice margin (Figure 6a). In comparison, the atmospheric heat transport is approximately 6 PW in years 91–100 (Figure 7).

[12] The total radiative forcing, the sum of the total solar radiation incident at the surface and the total long-wave radiation lost to the atmosphere, decreases by  $<40 \text{ Wm}^{-2}$  near the sea-ice margin (Figure 5) as a result of a reduction in cloud forcing by  $\sim 12 \text{ Wm}^{-2}$  (not shown) and the seasonal formation of sea ice. In this case, the reduction in cloud forcing is not sufficient to destabilize the sea-ice margin. In the control experiment, the total cloud forcing is large ( $\sim 15 \text{ Wm}^{-2}$ ) but varies over sea ice, land, and ocean (Figure 8). The total forcing over ocean is substantial and negative ( $-5 \text{ Wm}^{-2}$ ). In contrast, the cloud forcing over sea

ice is  $30 \text{ Wm}^{-2}$ . This large forcing arises because clouds over a high-albedo surface (ice) have a limited effect on planetary albedo, but a substantial greenhouse effect.

[13] To determine the climate sensitivity to a decrease in the radiative forcing, two experiments, FC\_92SL and FC\_91SL, were completed with 8 and 9% reductions in solar luminosity (Table 1). With a solar luminosity of 92% of modern, the global sea-ice fraction is nearly indistinguishable from the FC experiment. However, an additional 1% reduction in solar luminosity results in an ice-covered ocean after 57 years of model integration (not shown). The extreme sensitivity to a small change in forcing indicates the presence of a climate instability.

### 3.2. Slab-Ocean Implementation

[14] Previous experiments using FOAM have demonstrated that a fully coupled ocean-atmosphere model is less susceptible to a snowball Earth than a mixed layer ocean model due to differences in the treatment of ocean heat transport [Poulsen *et al.*, 2001]. To confirm this result, we

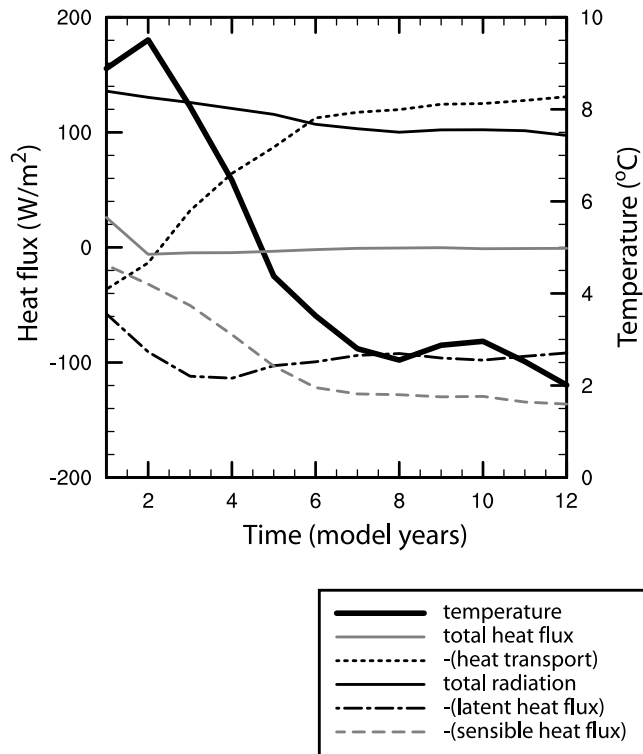


**Figure 5.** Evolution of the zonal average, surface ocean energy budget and zonal average sea-surface temperature ( $^{\circ}\text{C}$ ) at  $23^{\circ}\text{N}$  in the FC experiment. The  $23^{\circ}\text{N}$  latitude marks the equilibrium position of the sea-ice margin in the Northern Hemisphere. In this figure, negative heat flux represents loss from the surface ocean to the atmosphere; positive heat flux indicates heat gain to the surface ocean. As sea ice advances from the poles during the initial 12 years of simulation, the sensible heat loss increases but is partially compensated by increased ocean heat transport. As a result, the total heat flux is negative, and the sea-surface temperature decreases. The heat budget attains a balance (with total heat flux of  $0\text{ Wm}^{-2}$ ) shortly after year 12.

ran an experiment utilizing a 50-m slab-ocean model with no ocean heat transport. After 16 model years, sea ice covered the entire ocean (Figure 2b). The experiment was run for only 20 model years; the high albedo of sea ice prevents recovery from an ice-covered Earth. In contrast to experiments using the ocean GCM (the FC experiments), the slab-ocean model was initialized with warmer ocean temperatures ( $20^{\circ}\text{C}$  compared to  $0^{\circ}\text{C}$  at the surface) explaining the lag in sea-ice growth (Figure 2b).

[15] The prediction of global ice cover in the slab experiment is consistent with the results from previous atmospheric GCM experiments with mixed layer ocean implementations [Poulsen *et al.*, 2001]. This result indicates that the ocean plays a major role in weakening the ice albedo feedback, but does not provide specific insight into the model physics responsible for this behavior.

### 3.3. Shallow (86 m) Ocean

[16] The deep ocean may play a critical role in weakening the ice albedo feedback in the FC experiment through heat

transport by the large-scale overturning circulation. If this is the case, we would conclude that the FC result is not robust since the details of the Neoproterozoic bathymetry, continental distribution, initial conditions, and deep-ocean circulation will never be known with certainty.

[17] To test the influence of the deep ocean on the Neoproterozoic climate, a 100-year experiment was run with a uniform 86 m ocean using the ocean GCM. In the FC\_SHLW experiment, the sea-ice line stabilized at  $\sim 24^{\circ}$  latitude, approximately  $3^{\circ}$  equatorward of the sea-ice margin in the FC experiment (Figure 2c). In comparison to the FC experiment, the FC\_SHLW experiment has reduced ocean heat transport (Figures 6a and 6b) at low latitudes that is partially compensated by higher atmospheric heat transport (Figure 7). The reduction in ocean heat transport

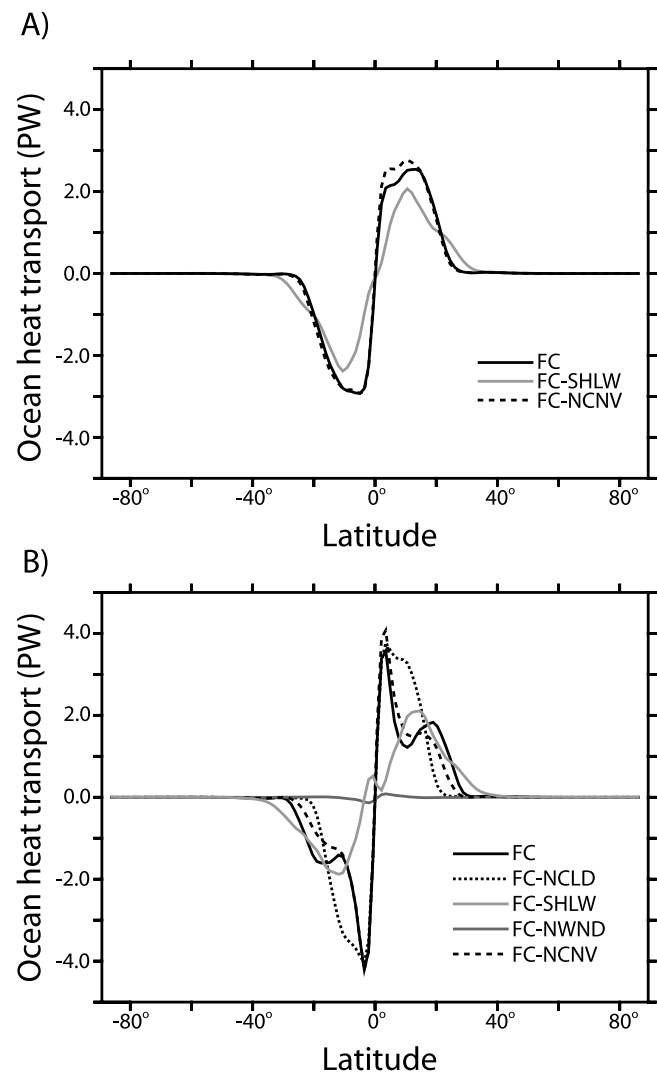


**Figure 6.** Mean annual, meridional, ocean heat transport (petawatts). (a) Mean annual ocean heat transport is displayed for model year 100 of the FC, FC\_SHLW, and FC\_NCNV experiments. (b) Mean annual ocean heat transport early in the model integration (model year 4). Note that the ocean heat transport is practically zero above  $30^{\circ}$  latitude because the ocean is covered with sea ice.

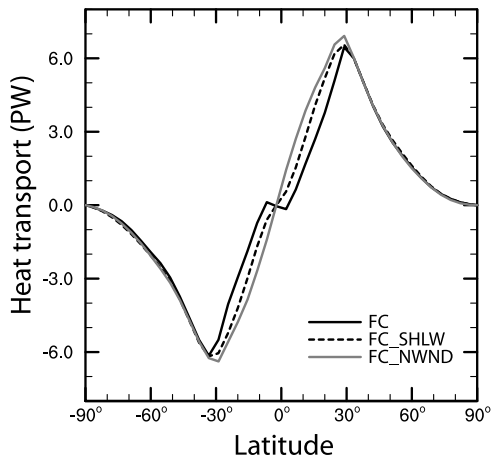


**Figure 7.** Mean annual, meridional, atmospheric heat transport (petawatts). Atmospheric heat transport is displayed for model year 100 of the FC and FC\_SHLW experiments, and model year 4 of the FC\_NWND experiment. In these years the sea-ice line is located at about the same latitude in each experiment.

arises from a reduction in the overturning circulation in a very shallow ocean. As a result of changes in ocean heat transport, low-latitude surface temperatures are higher (up to 5 °C) and subtropical temperatures are lower (Figure 9), facilitating a small expansion of sea ice.

[18] The FC\_SHLW experiment demonstrates that the deep ocean is important, but not critical, to weakening the ice albedo feedback. Moreover, this experiment suggests that long (1000 year) ocean GCM integrations are probably unnecessary to achieve sea-ice equilibrium, assuming that the initial ocean temperatures have been judiciously chosen.

### 3.4. Simple Sea-Ice Model

[19] In previous Neoproterozoic simulations using FOAM [Poulsen *et al.*, 2001, 2002], a simple nonthermodynamic sea-ice model was implemented. To directly test the influence of this simple sea-ice model on simulations of the Neoproterozoic, we ran the FC\_SICE experiment using the simple sea-ice model (Table 1). In comparison to the FC experiment, the global sea-ice fraction is significantly reduced (Figure 2b) and the sea-ice line stabilizes at higher latitudes ( $\sim 60^\circ$ ), indicating that the simple sea-ice model underestimates sea ice. Owing to the high-latitude position of the sea-ice line and our prior experimentation with the simple sea-ice model, the FC\_SICE experiment was integrated for only 40 years.

[20] The simple sea-ice model predicted sea ice with a constant thickness whenever the sea-surface temperature reached  $-1.92^\circ\text{C}$  and predicted ice-free ocean whenever the sea-surface temperature exceeded  $-1.92^\circ\text{C}$ . As demonstrated in the work of Poulsen *et al.* [2001] and in unpublished results, the simple sea-ice model does not prevent the simulation of global sea-ice coverage in FOAM. However, the simple sea-ice model does produce a switch-like behavior (ice on or off), resulting in large seasonal sea-ice fluctuations. More importantly, by ignoring seasonal

thickening of sea ice and the energy required to melt the ice, spring and summer sea-ice loss was overestimated, weakening the ice albedo feedback.

### 3.5. Buoyancy-Driven Ocean Convection

[21] Poulsen *et al.* [2001] and Bendtsen [2002] reported that convective energy release at the sea-ice margin weakened the ice albedo feedback, impeding sea-ice advance. In FOAM, a statically unstable condition in an ocean column triggers convective adjustment, which mixes adjacent grid cells to eliminate the buoyancy instability. If the buoyancy instability is due to temperature, the mixing between grid cells transfers heat from deeper levels to the surface level, warming the surface and weakening the ice albedo feedback [Poulsen *et al.*, 2001]. To explicitly test the effect of ocean convection on the sea-ice margin, the FC\_NCNV experiment was run without the convective adjustment parameterization.

[22] After 100 model years, the sea-ice line in the FC\_NCNV experiment stabilized at  $\sim 27^\circ$  latitude, nearly the same location as the sea-ice margin in the FC experiment. The global ice fraction is slightly larger than that in the FC experiment (Figure 2c). Sea-surface temperatures, particularly near the sea-ice margin, are lower without the surface heat contribution from convection mixing (Figure 9). However, ocean and atmospheric heat transports differ little between the FC\_NCNV and FC experiments (Figures 6 and 7). In sum, the convective adjustment parameterization is not responsible for inhibiting sea-ice expansion at low latitudes.

### 3.6. Wind-Driven Ocean Circulation

[23] The wind-driven circulation is an important mechanism for heat transport in the modern ocean [e.g., Wiffels *et*

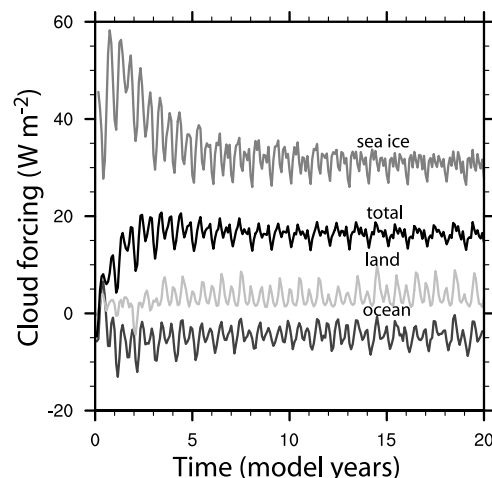


**Figure 8.** Cloud forcing ( $\text{Wm}^{-2}$ ) versus time (model years). The solid lines represent the cloud forcing over the total (black), ocean (dark gray), sea-ice (gray), and continental (light gray) surfaces simulated in the FC experiment. As the sea ice equilibrates, the global cloud forcing (total) stabilizes at approximately  $15 \text{ Wm}^{-2}$ . The cloud forcing is negative over the ocean but large and positive over sea ice.

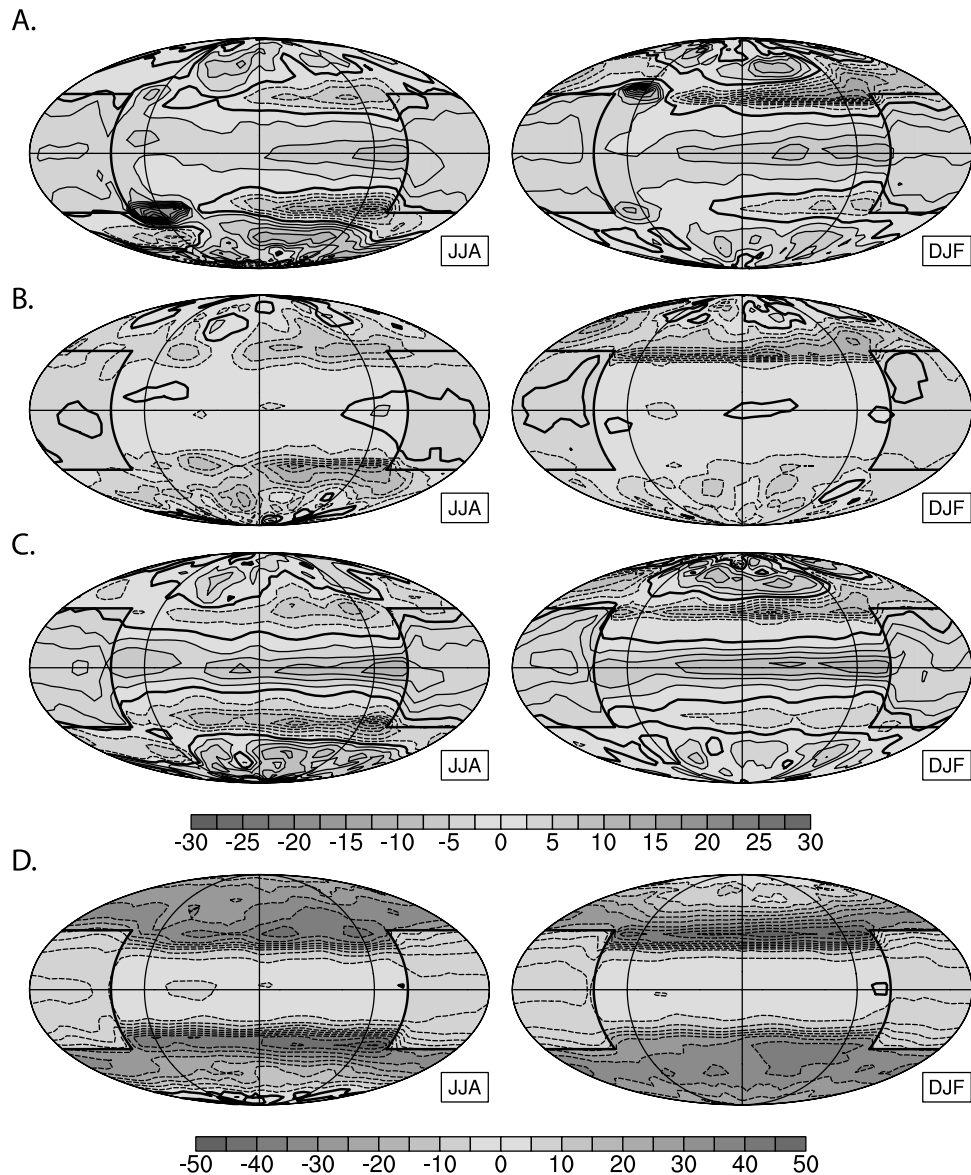


**Figure 9.** Snapshot of surface temperature difference ( $^{\circ}\text{C}$ ) from the control experiment, FC, averaged over December, January, and February (DJF) and June, July, and August (JJA). The following surface temperature differences are plotted: (a) FC\_SHLW-FC; (b) FC\_NCNV-FC; (c) FC\_NWND-FC; and (d) FC\_NCLD-FC. Results are shown for model year 4 to demonstrate how the surface energy balance differs between experiments early in their integration before sea ice reaches the low latitudes. In year 4 the experiments are not in equilibrium. The temperature differences shown here are meant to provide a snapshot of how the experiments are evolving. See text for further explanation. The Neoproterozoic continent is outlined by the thick, solid line. The contour interval is  $5^{\circ}\text{C}$ . See color version of this figure in the HTML.

*al.*, 1996], but is not explicitly resolved in most energy balance models and mixed layer atmospheric GCMs. In the FC\_NWND experiment, the wind stress at the sea surface was set to zero, effectively eliminating the wind-driven circulation.

[24] In the absence of wind-driven circulation, the sea ice advances to the equator, covering the entire ocean in less than 13 model years (Figure 2b). This result can be explained by the nearly complete absence of ocean heat transport (Figure 6). In the FC experiment, as the sea ice

advances and the sensible heat loss at the sea surface increases, heat is gained through ocean heat transport until a balance is attained and the sea-ice margin stabilizes (Figure 5). In the absence of ocean heat transport, the surface heat loss is greater than the gain, propelling the sea ice toward the equator. In comparison to the FC experiment, sea-surface temperatures are higher (greater than  $20^{\circ}\text{C}$ ) in low latitudes and colder in the subtropics in model year 4 (Figure 9), a pattern consistent with a reduction in ocean heat transport [Barron *et al.*, 1993]. In



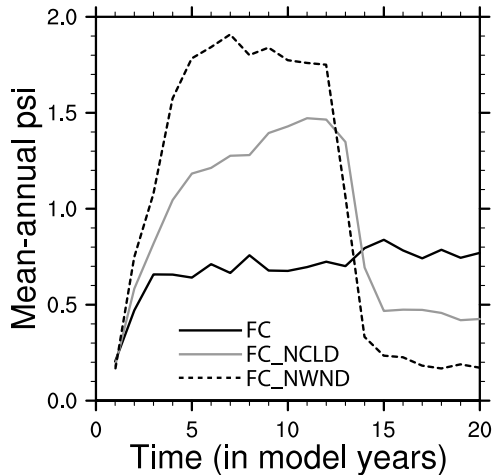


**Figure 10.** Mean annual, absolute maximum  $\psi$  ( $10^{10} \text{ kg}^{-1}$ ) versus time (model year). The absolute maximum  $\psi$  represents the absolute maximum value of the global mass stream function, which indicates the maximum intensity of the Hadley circulation. In the FC\_NCLD and FC\_NWND experiments the Hadley circulation intensifies abruptly as the sea ice advances into the low latitudes and weakens abruptly just prior to the complete freezing of the sea surface.

response to reduced heat transport and enhanced low-latitude thermal gradient, the atmospheric heat transport is greater in the FC\_NWND experiment than the FC experiment (Figure 7).

[25] In addition to the reduction in ocean heat transport, the ice albedo feedback is strengthened by a substantial increase in the mean annual Hadley circulation (Figure 10). The Hadley circulation increases as the temperature gradient within its domain increases. Both the absence of ocean heat transport and the migration of sea ice support the large thermal gradient. By model year 6, the maximum mass stream function was approximately three times greater than that in the FC experiment. The Hadley circulation works to decrease the temperature gradient within its domain, effectively increasing the sensible heat loss at the sea-ice margin promoting further sea-ice growth. The Hadley circulation collapses in year 12, when only a small zone of open ocean remains (Figure 10).

[26] The FC\_NWND experiment indicates that the wind-driven circulation is critical to preventing global sea-ice cover. The wind-driven circulation is an important mechanism for the ocean heat transport that is necessary to balance the surface energy budget near the sea-ice margin. In addition, through its control on the low-latitude thermal gradient, the wind-driven circulation influences the strength of the Hadley circulation and the advection of cold air from the sea-ice margin.

### 3.7. Cloud Forcing

[27] The treatment of clouds in Neoproterozoic modeling studies has been largely neglected. A systematic study of the role of clouds has not yet been undertaken and is not the objective of this study. However, to determine the gross

effect of clouds on the Neoproterozoic climate, a final experiment, FC\_NCLD, was conducted in which the cloud radiative forcing was turned off, eliminating the cloud contributions to planetary albedo and greenhouse effect.

[28] In the absence of cloud radiative forcing, the ocean is completely covered by sea ice by model year 14 (Figure 2b). Unlike the FC\_NWND experiment, the ocean heat transport in the FC\_NCLD experiment is substantial early in the model integration, approximately 3 PW (Figure 6). However, in the absence of a cloud forcing of  $30 \text{ Wm}^{-2}$  (Figure 8), air temperatures over sea-ice surfaces are considerably lower than those in the FC experiment (Figure 9). As a consequence, sea-surface sensible heat loss at the sea-ice margin increases, promoting cooling and strengthening the ice albedo feedback.

[29] As the sea ice advances into the Hadley domain, the mass stream function increases significantly (Figure 10) as a result of the increased meridional temperature gradient. As in the FC\_NWND experiment, the Hadley circulation acts to smooth the meridional temperature gradient, cooling seawater near the sea-ice margin and promoting further sea-ice growth. The Hadley circulation collapses in year 13 (Figure 10).

[30] Figures 11 and 12 illustrate the ocean and atmospheric heat transport during years 4, 6, 10, and 14 of the FC\_NCLD experiment. As the sea-ice advances and surface ocean temperatures cool to the freezing point, the ocean heat transport declines to nearly zero (Figure 11). Owing to the rapid advance of sea ice, ocean temperatures below the mixed layer have changed very little from initial conditions. The atmospheric heat transport also declines, but at a slower relative rate (Figure 12). Once the sea ice is within the Hadley domain, the heat transports are intimately linked; ocean heat transport acts to sustain a large thermal gradient at the sea-ice margin. Atmospheric heat transport works to diminish this gradient.

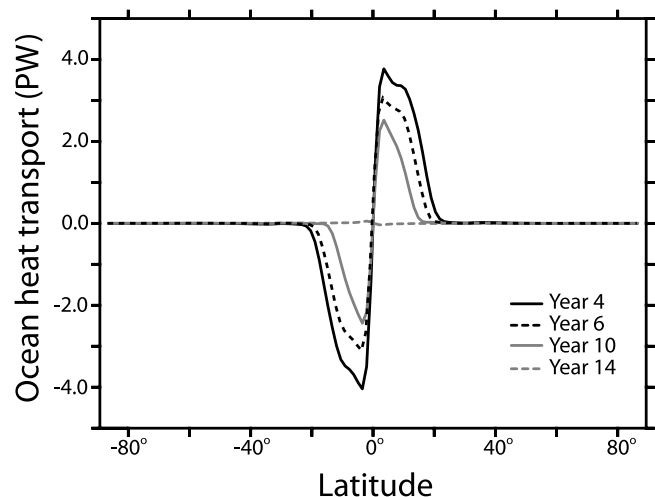


**Figure 11.** Mean annual, meridional ocean heat transport (PW) in years 4 (black line), 6 (black, dashed line), 10 (gray line), and 14 (gray, dashed line) of the FC\_NCLD experiment. The ocean heat transport diminishes to nearly zero as sea ice intrudes upon the low latitudes.

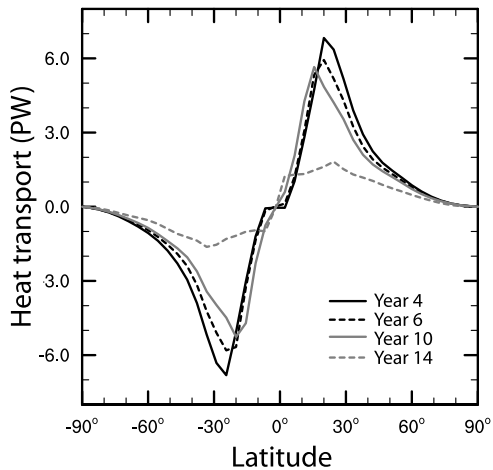


**Figure 12.** Mean annual, meridional atmospheric heat transport (PW) in years 4 (black line), 6 (black, dashed line), 10 (gray line), and 14 (gray, dashed line) of the FC\_NCLD experiment. The atmospheric heat transport declines as the thermal gradient lowers with the advance of sea ice into the low latitudes.

[31] These experimental results indicate that cloud forcing is also a critical factor that inhibits global ice cover. Clouds have a net positive forcing on the planet in FOAM. In their absence, global cooling ensues, strengthening the ice albedo feedback.

#### 4. Discussion

[32] In comparison to previously published modeling results, FOAM remains less susceptible to global sea-ice cover. In this study, we have attempted to determine the factors that inhibit global ice cover. The results from FOAM indicate that the wind-driven ocean circulation and cloud forcing play critical roles in the simulation of a snowball Earth through their influence on ocean and atmospheric heat transports. In the Neoproterozoic experiments, wind-driven circulation is the primary means of low-latitude ocean heat transport; in the absence of this ocean heat transport, the climate becomes unstable and sea ice grows to the equator. In FOAM, clouds contribute positively to the global radiative forcing; in the absence of this forcing, air temperature over sea ice is reduced, enhancing sensible heat loss at the sea-ice margin and cooling sea-surface temperatures. Both wind-driven circulation and cloud forcing act to weaken the ice albedo feedback.

[33] The wind-driven ocean circulation and clouds are treated very differently between climate models possibly explaining substantial model differences in response to Neoproterozoic conditions. Most energy balance models and mixed layer atmospheric GCMs either drive the upper ocean using some variant of modern zonal average wind forcing [e.g., Lewis *et al.*, 2003] or do not explicitly include wind-driven circulation. In either case, if the parameterized wind-driven ocean circulation is too small, it is likely that the ice albedo feedback is too strong. In fact, models that explicitly resolve the wind-driven ocean circulation demonstrate a

reduced susceptibility to snowball Earth [e.g., Poulsen *et al.*, 2001, 2002; Donnadieu *et al.*, 2004; this study]. Similarly, cloud treatment varies tremendously between climate models. Clouds are a major source of uncertainty in the modern climate [Intergovernmental Panel on Climate Change (IPCC), 2001] and in modeling studies as well. For better or worse, clouds are resolved in most atmospheric GCMs. The parameterization of cloud physics and radiative forcing can vary substantially between GCMs. In EBMs and intermediate complexity atmospheric models, clouds are not explicitly parameterized. Rather, the modern effects of clouds are frequently wrapped in an absorption coefficient that describes the absorption of heat in the atmosphere. In any case, it is likely that clouds contribute significantly to the disparity between climate models of the Neoproterozoic. It is important to note, however, that the greatest cloud forcing in the Neoproterozoic simulations occurs over sea ice. Because clouds over high-albedo surfaces are unlikely to substantially increase the planetary albedo, the radiative forcing will likely be large and positive in other GCMs with different cloud physics implementations.

[34] The Hadley circulation influences the ice albedo instability. Through atmospheric heat transport, the Hadley circulation reduces the thermal gradient in the low latitudes and delivers energy to the sea-ice margin, working against the ice albedo feedback [Lindzen and Farrell, 1977; Bendtsen, 2002; Donnadieu *et al.*, 2004]. However, once sea ice enters the Hadley domain, the Hadley circulation works to reduce the meridional thermal gradient through advection, cooling seawater near the sea-ice margin and strengthening the ice albedo feedback [Bendtsen, 2002]. The magnitude of this feedback will depend on the Hadley cell intensity. Our results indicate that the advance of sea ice into the Hadley domain significantly increases the strength of the mean annual Hadley circulation, which then further enhances the ice albedo feedback. Interestingly, the Hadley circulation collapses prior to complete freezing of the ocean surface, weakening the ice albedo feedback. Under certain conditions, the collapse of the Hadley circulation might allow for a limited sea ice-free region near the equator.

[35] The addition of a thermodynamic sea-ice model in FOAM caused a substantial increase in the simulation of sea ice and a reduction in the seasonal sea-ice fluctuation. Without the thermodynamic barrier to sea-ice melt, as in the simple sea-ice model implementation of FOAM, sea ice disappeared when the sea-surface temperature exceeded the seawater freezing point. With a thermodynamic sea-ice model, the melting of thick sea-ice formed during the winter requires substantial energy in the spring and summer reducing the seasonal melting and enhancing the sea-ice expanse. Using a simple sea-ice model, Poulsen *et al.* [2001] reported that convective mixing at the sea-ice margin stopped sea-ice advance into midlatitudes, but suggested that other ocean mechanisms would be important if sea ice advanced to the low latitudes. Neoproterozoic experiments confirm this prediction and demonstrate that wind-driven circulation controls ocean heat transport at low latitudes.

[36] Was there a snowball Earth in the late Neoproterozoic? To date, geologists strongly disagree on the interpretation of the geological record (see the differing

interpretations in Hoffman and Schrag [2002], Ridgwell *et al.* [2003], Eyles and Januszczak [2004], and Jiang *et al.* [2003]). Climate modeling efforts have also failed to reach a consensus and for good reason. The models used to simulate Neoproterozoic climate have differed tremendously in their formulations and capabilities. To our knowledge, a climate model does not currently exist that incorporates all of the climate components including dynamic atmosphere, ocean, sea ice, and ice sheet submodels, necessary to adequately simulate the Neoproterozoic climate. FOAM is no exception and currently does not include dynamic sea-ice, or marine or continental ice sheet submodels that might influence the climate sensitivity to Neoproterozoic conditions. Even if such a model existed, uncertainties in the Neoproterozoic boundary conditions and model parameterizations would probably allow for a wide range of solutions. At this stage in the modeling of Neoproterozoic climate, model results should not be used to argue one way or another for the existence of a Neoproterozoic snowball Earth. Rather, climate models should be used to gain insights into the processes or mechanisms that might contribute to promoting or inhibiting global sea-ice cover.

## 5. Summary

[37] The objective of this study was to determine the factors that inhibit global sea-ice cover in coupled ocean-atmosphere simulations of the Neoproterozoic. A series of

experiments were undertaken to systematically evaluate the effect of the deep-ocean circulation, wind-driven ocean circulation, convective mixing, sea-ice treatment, and radiative cloud forcing, on snowball Earth simulation. Two factors, wind-driven ocean circulation and cloud radiative forcing, were found to inhibit the simulation of a snowball Earth in FOAM. Because the wind-driven ocean circulation and (positive) cloud radiative forcing over sea ice are unlikely to be model dependant, we expect these factors are important controls on global sea-ice simulation in other ocean-atmosphere GCMs. In the absence of either the wind-driven ocean circulation or cloud radiative forcing, a snowball Earth solution was rapidly simulated. In addition, the Hadley circulation was demonstrated to influence the ice albedo feedback. These model results underscore the importance of atmosphere and ocean dynamics to the ice albedo feedback, and provide insights into the wide disparity between previously reported modeling results. Owing to uncertainties in model parameterizations and boundary conditions and the absence of potentially important subcomponents, these results should not be used to argue one way or another for a snowball Earth during the late Neoproterozoic.

[38] **Acknowledgments.** All climate experiments were completed using the advanced computing resources at the University of Michigan Paleoclimate Modeling Lab. We thank L. Sloan and two reviewers for their constructive comments.

## References

- Barron, E. J., W. H. Peterson, D. Pollard, and S. Thompson (1993), Past climate and the role of ocean heat transport: Model simulations for the Cretaceous, *Paleoceanography*, *8*, 785–798.
- Bendtsen, J. (2002), Climate sensitivity to changes in solar insolation in a simple coupled climate model, *Clim. Dyn.*, *18*, 595–609.
- Chandler, M. A., and L. E. Sohl (2000), Climate forcings and the initiation of low-latitude ice sheets during the Neoproterozoic Varanger glacial interval, *J. Geophys. Res.*, *105*, 20,737–20,756.
- Crowley, T. J., and S. K. Baum (1993), Effect of decreased solar luminosity on Late Precambrian ice extent, *J. Geophys. Res.*, *98*, 16,723–16,732.
- Donnadieu, Y., G. Ramstein, F. Fluteau, D. Roche, and A. Ganopolski (2004), The impact of atmospheric and oceanic heat transports on the sea-ice-albedo instability during the Neoproterozoic, *Clim. Dyn.*, *22*, 293–306.
- Drake, J., I. Foster, J. Michalakes, B. Toonen, and P. Worley (1995), Design and performance of a scalable parallel community climate model, *Parallel Comput.*, *21*, 1571–1591.
- Eyles, N., and N. Januszczak (2004), ‘Zipper rift’: A tectonic model for Neoproterozoic glaciations during the breakup of Rodinia after 750 Ma, *Earth Sci. Rev.*, *65*, 1–73.
- Hoffman, P. F., and D. P. Schrag (2002), The snowball Earth hypothesis: Testing the limits of global change, *Terra Nova*, *14*, 129–155.
- Hoffman, P. F., A. J. Kaufman, G. P. Halverson, and D. P. Schrag (1998), A Neoproterozoic snowball earth, *Science*, *281*, 1342–1346.
- Hyde, W. T., T. J. Crowley, S. K. Baum, and W. R. Peltier (2000), Neoproterozoic “snowball Earth” simulations with a coupled climate/ice-sheet model, *Nature*, *405*, 425–429.
- Intergovernmental Panel on Climate Change (IPCC) (2001), *Climate Change 2001: The Scientific Basis, Contribution of Working Group 1 to the Third Assessment Report of the Intergovernmental Panel on Climate Change*, edited by J. T. Houghton *et al.*, 881 pp., Cambridge Univ. Press, New York.
- Jacob, R. (1997), Low frequency variability in a simulated atmosphere ocean system, Ph.D. thesis, 159 pp., Univ. of Wisc., Madison.
- Jiang, G., M. J. Kennedy, and N. Christie-Blick (2003), Stable isotopic evidence for methane seeps in Neoproterozoic postglacial cap carbonates, *Nature*, *426*, 822–826.
- Kennedy, M. J., N. Christie-Blick, and L. E. Sohl (2001), Are Proterozoic cap carbonates and isotopic excursions a record of gas hydrate destabilization following Earth’s coldest intervals?, *Geology*, *29*, 443–446.
- Kiehl, J. T., J. J. Hack, G. B. Bonan, B. A. Boville, B. P. Briegleb, D. L. Williamson, and P. J. Rasch (1996), Description of the NCAR Community Climate Model (CCM3), *NCAR Tech. Note NCAR/TN-420+STR*, 152 pp., Natl. Cent. for Atmos. Res., Boulder, Colo.
- Kirschvink, J. L. (1992), Late Proterozoic low-latitude global glaciation: The snowball Earth, in *The Proterozoic Biosphere*, edited by J. W. Schoff and C. Klein, pp. 51–52, Cambridge Univ. Press, New York.
- Lewis, J. P., A. J. Weaver, S. T. Johnston, and M. Eby (2003), Neoproterozoic “snowball Earth”: Dynamic sea ice over a quiescent ocean, *Paleoceanography*, *18*(4), 1092, doi:10.1029/2003PA000926.
- Lindzen, R. S., and B. Farrell (1977), Some realistic modifications of simple climate models, *J. Atmos. Sci.*, *34*, 1487–1501.
- Marshall, H. G., J. C. G. Walker, and W. R. Kuhn (1988), Long-term climate change and the geochemical cycle of carbon, *J. Geophys. Res.*, *93*, 791–801.
- Poulsen, C. J. (2003), Absence of a runaway ice-albedo feedback in the Neoproterozoic, *Geology*, *31*, 473–476.
- Poulsen, C. J., R. T. Pierrehumbert, and R. L. Jacob (2001), Impact of ocean dynamics on the simulation of the Neoproterozoic “snowball Earth,” *Geophys. Res. Lett.*, *28*, 1575–1578.
- Poulsen, C. J., R. L. Jacob, R. T. Pierrehumbert, and T. T. Huynh (2002), Testing paleogeographic controls on a Neoproterozoic snowball Earth, *Geophys. Res. Lett.*, *29*(11), 1515, doi:10.1029/2001GL014352.
- Ridgwell, A. J., M. J. Kennedy, and K. Caldiera (2003), Carbonate deposition, climate stability, and Neoproterozoic ice ages, *Science*, *302*, 859–862.
- Semtner, A. J. (1976), A model for the thermodynamic growth of sea ice in numerical investigations of climate, *J. Atmos. Sci.*, *6*, 379–389.
- Wijffels, S. E., J. M. Toole, H. L. Bryden, R. A. Fine, W. J. Jenkins, and J. L. Bullister (1996), The water masses and circulation at 10°N in the Pacific, *Deep Sea Res.*, *43*, 501–544.

R. L. Jacob, Argonne National Laboratory, Argonne, IL 60439, USA.

C. J. Poulsen, Department of Geological Sciences, University of Michigan, Ann Arbor, MI 48109, USA. (poulsen@umich.edu)